

Transition to turbulence in suspension Taylor-Couette flow

Meheboob Alam^{2,*} and Manojit Ghosh^{1,**}

¹Engineering Mechanics Unit, Jawaharlal Nehru Centre for Advanced Scientific Research, Jakkur P.O, Bengaluru 560064, India.

Abstract. The pattern transition routes to turbulence are explored via experiments in a Taylor-Couette setup for neutrally-buoyant suspensions of non-colloidal particles in the counter-rotation regime. For small counter-rotations, the super-critical bifurcation scenario holds, leading to turbulent Taylor vortices (TTV) that are characterized by large-scale stationary toroidal rolls in the background of small-scale structures. At strong counter-rotations, however, the primary bifurcation is sub-critical, leading to spiral vortices, and the final bifurcating state represents a featureless turbulent (TUR) state, devoid of large-scale structures. The spectral routes towards TTV and TUR are analysed, and compared with particle-free cases to infer possible roles of inertial particles.

1 Introduction

According to Landau-Hopf [1, 2] conjecture, the laminar flow undergoes an infinite sequence of bifurcations with increasing Reynolds number, resulting in increasing degrees of spatio-temporal complexities before the turbulent motion sets in; the complexities are thought to be characterized by the appearance of new frequencies (f_1, f_2, \dots, f_k) such that they are not rationally tied to each other (i.e., $f_j/f_k \neq m/n$, with $m, n \in \mathcal{N}$, for $j \neq k$), leading to a complicated “quasi-periodic” motion in the phase space. This theory was subsequently replaced by the Ruelle-Takens scenario [3] that advocates the appearance of a finite number of Hopf bifurcations before the flow could degenerate into a “strange attractor” [4, 5]. Ruelle and Takens’s work established two key ideas: (i) the transition scenario conjectured by Landau and Hopf is not generic, and (ii) an open set of strange attractors exists in the vicinity of any quasi-periodic flow involving at least four oscillatory modes. Since 1975 [4], the quasi-periodic transition route has been verified in a variety of experiments for which the Taylor-Couette flow (TCF, the annular flow between two differentially-rotating co-axial cylinders [6, 7]) has served as a model system that admits a sequence of bifurcations [8–11] leading to turbulent states [4, 12–14].

In the context of multiphase flows (such as in liquid-solid suspensions), not much work has been done to understand the role of inertial particles [15–18] in mediating the transition-routes to turbulence in dilute-to-dense particulate suspensions that are characterized by shear-thinning and shear-thickening rheology [19]. For neutrally-buoyant non-colloidal particle suspensions, the TCF has been studied during the last seven years via experiments [20–25], linear stability theory [26] and numerical simulation [27]. Collectively, these works confirmed that the

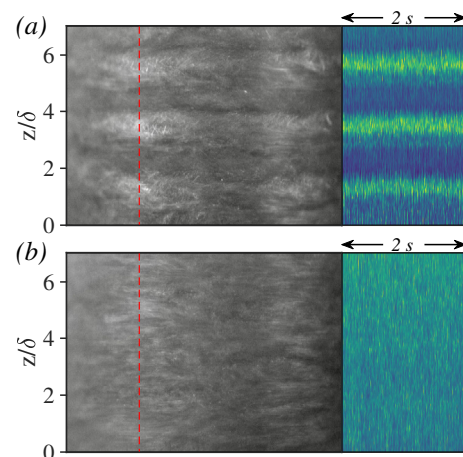


Figure 1. States of (a) turbulent Taylor vortex (TTV) at $\Omega = -0.5$ and $Re_s = 2227.8$ and (b) featureless turbulence (TUR) at $\Omega = -1$ and $Re_s = 2539.4$. Both panels refer to the particle-free ($\phi = 0$) Newtonian fluid; the left and right parts represent an image and its space-time map (over 2 s), respectively.

critical Reynolds number for first bifurcation decreases monotonically with increasing particle loading. The second finding is that the primary bifurcating state could be a non-axisymmetric travelling wave [20, 21] if the particle volume fraction exceeds a minimum value (about 5–10%): (i) a spiral vortex flow (SVF), or, a ribbon (RIB, a coexisting state of left- and right-handed spirals, [20]), or, (ii) a coexisting state of TVF and SVF or WTV (wavy Taylor vortex) [21].

While all prior works on suspension TCF [20–27] belong to the case with a rotating inner cylinder and a stationary outer cylinder (i.e., the rotation ratio is $\Omega = \omega_o/\omega_i = 0$), the present group [28–30] explored the pattern transition scenario with both cylinders rotating. The reason for studying the counter-rotation regime ($\Omega \leq 0$) is that

*e-mail: meheboob@jncasr.ac.in

**e-mail: mathmanojit@gmail.com

two distinct turbulent states [8, 9] are known to exist for Newtonian fluids, see Figs. 1(a) and 1(b) that represent TTV (a turbulent state against the background of large-scale Taylor vortices) and TUR (a featureless turbulent state, characterized by small-scale structures) states, respectively. How these two turbulent states are reached as the differential rotation rate is increased is the focus of this work with suspension TCF.

2 Experiments with suspension TCF

The suspension is prepared by homogeneously mixing neutrally buoyant, rigid PMMA microspheres, having a mean diameter $d_p \approx 50 \mu\text{m}$, with a Newtonian solvent [21] such that the suspension is density matched ($\rho_{\text{solvent}} = \rho_p \approx 1190 \text{ kg/m}^3$). The measured viscosity $\mu(\phi)$ of the suspension is found to follow the Krieger–Dougherty relation $\mu(\phi) = \mu(0)(1 - \phi/\phi_m)^{-2}$, where $\mu(0) \approx 7.9 \text{ mPa s}$ is the solvent viscosity at $T = 22^\circ\text{C}$, $\phi_m = 0.585$ is the maximum packing fraction, and $\mu_r(\phi) = \mu(\phi)/\mu(0) \geq 1$ is the relative viscosity [19] of the suspension.

Our Taylor-Couette (TC) cell has an aspect ratio of $\Gamma = h/\delta \approx 8.46$ and a radius ratio of $\eta = r_i/r_o \approx 0.89$, where $h = 16.5 \text{ mm}$ is the height of the inner cylinder and $\delta = r_o - r_i$ is the gap width, with $r_i = 16 \text{ mm}$ and $r_o = 17.95 \text{ mm}$ being the radii of the inner and outer cylinders, respectively. This TC-cell is mounted on a rheometer (MCR-702, Anton Paar GmbH) having two independently rotating motors that are connected to the inner and outer cylinders; two motors are operated by specifying the rotation ratio,

$$\Omega = \omega_o/\omega_i = f_o/f_i, \quad (1)$$

of two cylinders, followed by quasi-static ramping protocols to increase/decrease the individual frequencies (f_o, f_i). The ramping rate is set to $|dRe(\phi)/d\tau| = 0.05/\mu_r(\phi)$ [30], where $Re(\phi) = \max\{Re_i(\phi), Re_o(\phi)\}$ and

$$Re_i(\phi) = \rho r_i \omega_i \delta / \mu(\phi) \quad \text{and} \quad Re_o(\phi) = \rho r_o \omega_o \delta / \mu(\phi) \quad (2)$$

are the inner and outer Reynolds numbers, respectively, and $\tau = t/\tau_{\text{vis}}$, with $\tau_{\text{vis}} = \rho \delta^2 / \mu(\phi)$ being the viscous diffusion time.

The maximum particle Reynolds number is estimated as $Re_p(\Omega) = \rho \dot{\gamma}_{\text{app}} d_p^2 / \mu(0) = Re_i^{\text{max}} |1 - \Omega/\eta| (d/\delta)^2 = O(2)$ at $\Omega = (-0.5, -1.0)$. The corresponding particle Stokes number $St_p = m_p \dot{\gamma}_{\text{app}} / (3\pi\mu(0)d_p)$ and Péclet number $Pe = 3\pi\mu(0)d_p^3 \dot{\gamma}_{\text{app}} / (4k_B T)$ are estimated as $O(0.1)$ and $O(10^9)$, respectively. Thus, the working fluid can be treated as a suspension of non-colloidal particles with considerable particle inertia $Re_p = O(1)$.

We will present flow visualization results for which the continuous video images of surface flow patterns are captured by a Nikon (D750 DSLR) camera at a frame rate of 60 s^{-1} . The images at a frame rate of 200 s^{-1} , using a high-speed (Phantom v9) camera, are also procured (over small time windows) to ascertain high-frequency modes [30].

3 Results and discussion

For specified values of (Ω, ϕ) , the pattern transition routes to turbulence is analysed by increasing the value of the

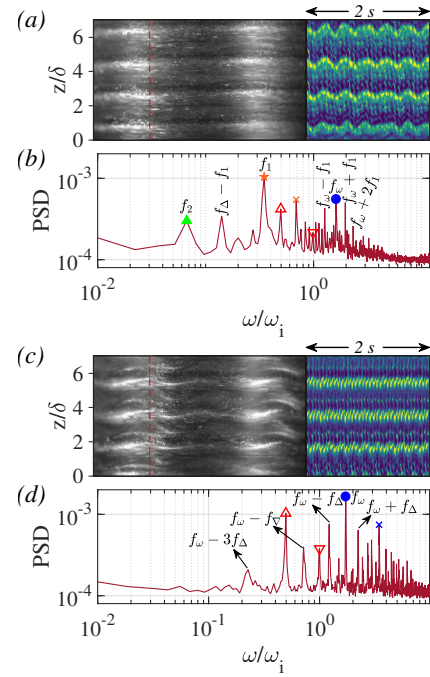


Figure 2. (a,b) A new quasi-periodic state of modulated wavy vortices (MWV₁) state at $Re_s = 395.65$; (c,d) wavy Taylor vortex (WTV) state at $Re_s = 478.30$, with $\phi = 0$ and $\Omega = -0.5$. Frequency peaks marked by open-red triangles and inverted triangles denote the frequencies of the outer and inner cylinders, respectively; see the text for details.

shear Reynolds number [12, 28–30]:

$$Re_s(\phi) = 2(1 + \eta)^{-1} |1 - \Omega| Re_i(\phi). \quad (3)$$

Below we present results for two rotation ratios of $\Omega = -0.5$ and -1.0 for which the final states are TTV and TUR, respectively, as shown in Figs. 1(a) and 1(b), respectively, for the particle-free case. It is clear from the space-time maps in Fig. 1 that the TTV state is characterized by large-scale Taylor vortices, while the TUR state is devoid of large-scale structures.

3.1 New quasi-periodic state and transition to TTV

For the particle-free case ($\phi = 0$) at $\Omega = -0.5$, the primary bifurcation from the circular Couette flow (CCF) is known to be super-critical and pitchfork, resulting in a stationary state of the well-known Taylor vortices [7–9] – these are toroidal vortices stacked along the axes of the cylinders, called the Taylor vortex flow (TVF, not shown). We have verified that the primary bifurcation at $\Omega = -0.5$ is CCF→TVF in present experiments [28] too at $\phi = 0$. Interestingly, the secondary bifurcation from TVF leads to two distinct time-dependent states: (i) WTV (wavy Taylor vortices) and (ii) MWV₁ (modulated wavy vortices). The latter is, in fact, a quasi-periodic state, see Fig. 2(a) for a snapshot (left panel) and the space-time evolution of a vertical strip (marked by the red line on the left panel) over 2 s in its right panel. It is clear from the space-time plot that the MWV₁ state is characterized by the presence

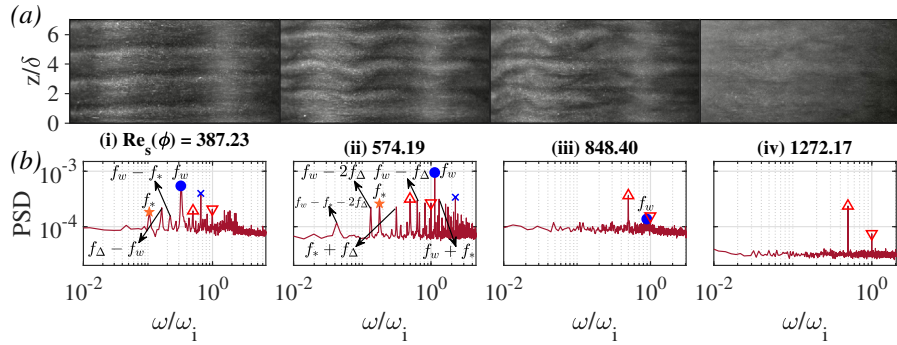


Figure 3. Transition to turbulent Taylor vortex (TTV) for $\phi = 0.15$ and $\Omega = -0.5$: (a) snapshots and (b) power spectra; (i) MWV_1 (new modulated wavy vortices), (ii) MWV (modulated wavy vortices), (iii) CWV (chaotic wavy vortices) and (iv) TTV.

of finite-amplitude, low frequency (f_2), modulations of the underlying wavy mode. The power-spectra in Fig. 2(b) indicates the presence of two frequencies (f_1 and f_2 , marked by the magenta star and green triangle, respectively) in addition to the wavy vortex mode (marked by the blue circle). Since f_1/f_2 and f_i/f_w are not rational numbers, Fig. 2(a,b) indeed represents a quasi-periodic state (QP_2) with two incommensurate frequencies. It may be noted that the quasi-periodic motion with three (QP_3) or four (QP_4) incommensurate frequencies are known to be unstable and hence may not be realizable in experiments.

The distinction of MWV_1 from the WTV state can be ascertained from Fig. 2(c,d) for $\phi = 0$. The PSD plot in Fig. 2(d) confirms the presence of a single frequency (marked the blue circle), representing the azimuthal propagation frequency of the wavy vortices. These waves can be identified with the undulations of the Taylor vortices as seen on the snapshot in Fig. 2(c)

The direct transition to quasi-periodic MWV_1 state was discovered in our previous work [28] at $\Omega = -0.5$ in a pure fluid ($\phi = 0$), and we confirmed its persistence for all particle loadings $\phi \leq 0.3$ in the present work. Our second finding is that the WTV mode does not exist at $\Omega = -0.5$ in the presence of particles ($0.05 \leq \phi \leq 0.3$) for which the secondary bifurcation, $CCF \rightarrow TVF \rightarrow MWV_1$, directly leads to a new quasi-periodic state. Note that the primary bifurcation at $\phi \geq 0.1$ is a non-axisymmetric mode (SVF) at $\Omega = -0.5$ [28, 29], resulting in a bifurcation sequence of $CCF \rightarrow SVF \rightarrow TVF \rightarrow MWV_1$ at $\phi \geq 0.1$.

Figure 3 displays a sequence of (a) snapshots and (b) their power spectra with increasing $Re_s(\phi)$ for a suspension with $\phi = 0.15$. The MWV_1 state and its PSD [Fig. 3(a,b)i] look similar to that for the particle-free case in Fig. 2(a,b); in addition to incommensurate frequencies, the MWV_1 state is characterised by a “decaying” tail of its PSD in both particle-free and particle-laden cases. With increasing Re_s , the MWV_1 gives birth to another quasi-periodic state of the standard MWV [10, 11]. Two key differences between MWV_1 and MWV are (i) $f_{MWV_1}^* \ll f_{MWV}^*$ and (ii) the PSD of MWV has a “flat-tail” [compare Figs. 3b(ii) and 3b(i)] with several high-frequency peaks.

The band of high-frequency peaks in MWV gradually disappears, leading to the emergence of a PSD with a “broad-tail” [Fig. 3b(iii)] which is a signature of

chaos [9, 10]. Note that the corresponding PSD plot contains a well-defined frequency peak (marked by the blue circle) that represents the propagation frequency of the background wavy vortices – this state is called CWV (chaotic wavy vortices) [10, 11]. The power/height of the CWV frequency-peak decreases gradually with increasing $Re_s(\phi)$, eventually yielding a statistically “stationary” turbulent state [Fig. 3b(iv)] with large-scale Taylor vortices – this is called TTV (turbulent Taylor vortices).

The above overall transition sequence beyond the MWV_1 state, $MWV_1 \rightarrow MWV \rightarrow CWV \rightarrow TTV$, is found to be similar in the particle-free ($\phi = 0$, not shown) case.

3.2 Transition to TUR at $\omega_i = -\omega_o$

For the exact counter-rotation case ($\omega_i = -\omega_o$, i.e., $\Omega = -1$), the primary bifurcation is known to be subcritical [8, 9], $CCF \rightarrow SVF$, leading spiral vortices (SVF, an axially propagating and azimuthally rotating helical mode). The subcritical nature of $CCF \rightarrow SVF$ bifurcation at $\Omega = -1$ has been verified from present torque measurements (not shown).

Figure 4(a) displays a sequence of space-time maps with increasing Re_s for $\phi = 0.15$, and the corresponding power spectra are shown in Fig. 4(b). Figure 4a(i) represents a down-ward propagating spiral (i.e., a right-handed spiral) which, on increasing Re_s , gives birth to another propagating state in which the left and right spirals penetrate axially, called “interpenetrating spiral vortices” (ISV) [9, 28]. The space-time map in Fig. 4a(ii) confirms that the up- and down-propagating spirals meet at around the mid-height ($z/\delta \approx 4$) of the TC cell, and both spirals propagate at the same frequency f_s [marked by the blue circle in Fig. 4b(ii)].

With increasing Re_s , the spirals penetrate into each other, resulting in a low-frequency incommensurate mode [28], and therefore the “nonlinear” ISV is a quasi-periodic state. Both frequency peaks become shallower with further increasing Re_s , eventually resulting in a stationary state as depicted in Fig. 4(a,b)(iii) – this is called “non-propagating interpenetrating spirals” (NIS [28]) whose space-time map resembles typical ‘spatio-temporal’ chaos. We have identified a distinguishing spectral characteristic of NIS: the tail of the power

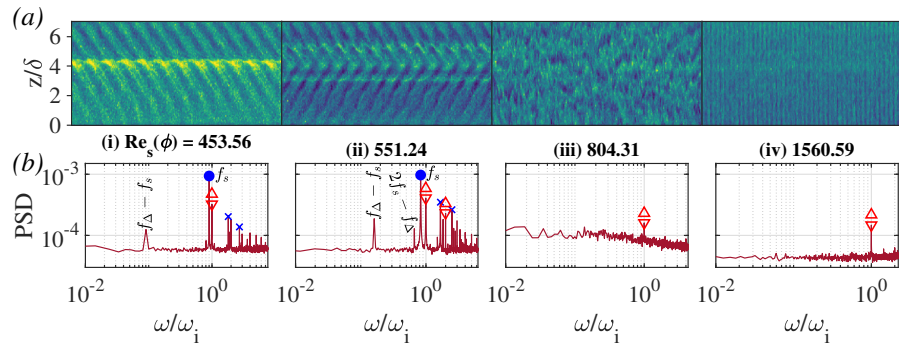


Figure 4. Transition to featureless turbulence (TUR) for $\phi = 0.15$ and $\Omega = -1.0$: (a) space-time maps (over 1 s) and (b) power spectra; (i) SVF (spiral vortex flow), (ii) ISV (interpenetrating spiral vortices), (iii) NIS (non-propagating interpenetrating spirals) and (iv) TUR.

spectra of the scattered light intensity follows a power-law decay, $\mathcal{P}(f) \sim f^{-\beta}$, as confirmed from the PSD-plot in Fig. 4b(iii). The vanishing of the exponent $\beta(Re_s) \rightarrow 0$ with increasing shear Reynolds number $Re_s(\phi)$, signifying the onset of the “flat” broadband tail [Fig. 4b(iv)] of $\mathcal{P}(f) \sim f^0$, has been tied to the onset of TUR. The latter is devoid of large-scale structures, see Fig. 4a(iv), and hence TUR represents a featureless turbulent state.

In summary, the origin of TUR at $\Omega = -1$ is tied to a sub-critical primary bifurcation, leading to spiral vortex flow (SVF), which undergoes a sequence of bifurcations, $CCF \rightarrow SVF \rightarrow ISV \rightarrow NIS \rightarrow TUR$, followed by (i) a quasi-periodic state (nonlinear ISV), (ii) a ‘stationary’ chaotic state (NIS) and (iii) a featureless turbulent state (TUR).

4 Conclusion and outlook

The pattern transition routes to TTV and TUR are found to be similar in both particle-free and particle-laden ($\phi \leq 0.3$) TCF [31, 32], except the appearance of non-axisymmetric primary modes (SVF/RIB) at $\phi > 0.05$ [20, 21]. The major qualitative differences appear in terms of (i) the structural modulations of patterns [20–25] (ii) the internal flow structure (shear-band-type velocity field in CCF state, anharmonicity of Taylor vortices, etc.) [21], (iii) the scaling of frequencies of various propagating modes [28, 30], and (iv) the (anomalous) torque responses in different states [21, 22, 25, 29]. Some of the latter results [29] are discussed in a companion paper [33].

References

[1] L.D. Landau, *Dokl. Akad. nauk SSSR* **44**, 311 (1944)
 [2] E. Hopf, *Commun. Appl. Maths.* **1**, 303-322 (1948)
 [3] D. Ruelle, F. Takens, *Commun. Math. Phys.* **20**, 167–192 (1971)
 [4] J. Gollub, H. Swinney, *Phys. Rev. Lett.* **35**, 927 (1975)
 [5] A. Brandstater, H. Swinney, *Phys. Rev. A* **35**, 2207 (1987)
 [6] M. Couette, *Comptes Rendus* **107**, 388–390 (1888)
 [7] G.I. Taylor, *Phil. Tran. Soc. A* **223**, 289–343 (1923)
 [8] D. Coles, *J. Fluid Mech.* **21** (3), 385–425 (1965)
 [9] C. Andereck *etal.* *J. Fluid Mech.* **164**, 155–183 (1986)

[10] Y. Takeda, *J. Fluid Mech.* **389**, 81–99 (1999)
 [11] C. Dutcher, S. Muller, *J. Fluid Mech.* **641**, 85 (2009)
 [12] B. Dubrulle *etal.*, *Phys. Fluids* **17**, 095103 (2005)
 [13] S. Grossmann, D. Lohse, C. Sun, *Annu. Rev. Fluid Mech.* **48**, 53–80 (2016)
 [14] D. Feldmann *etal.*, *Phil. Tran. R. Soc. A* **381** (2246), 20220114 (2023)
 [15] R.A. Bagnold, *Proc. R. Soc. A* **225**, 49–63 (1954)
 [16] J.P. Matas, J.F. Morris, E. Guazzelli, *Phys. Rev. Lett.* **90**, 014501 (2003)
 [17] L. Brandt, F. Coletti, *Annu. Rev. Fluid Mech* **22**, 159–189 (2022)
 [18] M. Hunt, R. Zenit, *Int. J. Mult. Flow* **180**, 104919 (2024)
 [19] E. Guazzelli, O. Pouliquen, *J. Fluid Mech.* **852**, P1 (2018)
 [20] M.V. Majji, S. Banerjee, J.F. Morris, *J. Fluid Mech.* **835**, 936–969 (2018)
 [21] P. Ramesh, S. Bharadwaj, M. Alam, *J. Fluid Mech.* **870**, 901–940 (2019)
 [22] A. Dash, A. Anantharaman, C. Poelma, *J. Fluid Mech.* **903**, A20 (2020)
 [23] P. Ramesh, Alam, *Phys. Rev. Fluids* **5**, 042301 (2020)
 [24] L. Baroudi, M.V. Majji, J.F. Morris, *Phys. Rev. Fluids* **5**, 114303 (2020)
 [25] M. Moazzen, T. Lacassagne, V. Thomy, S. Bahrani, *J. Fluid Mech.* **937**, A2 (2022)
 [26] J. Gillissen, H. Wilson, *Phys. Rev. Fluids* **4**, 044301 (2019)
 [27] C. Kang, P. Mirbod, *J. Fluid Mech.* **916**, A12 (2021)
 [28] S. Singh, M. Ghosh, M. Alam, *J. Fluid Mech.* **944**, A18 (2022)
 [29] M. Alam, M. Ghosh, *Phil. Trans. Roy. Soc. A* **381** (2243) 20220226 (2023)
 [30] M. Ghosh, M. Alam, *J. Fluid Mech.* **995**, R4 (2024)
 [31] M. Ghosh, M. Alam, “Routes to turbulent Taylor vortices: vortex splitting and merging in chaotic state and the role of particles”, *J. Fluid Mech.* (in revision, 2025a)
 [32] M. Ghosh, M. Alam, “Direct transition to chaos and turbulence in suspension Taylor-Couette flow”, *Preprint* (2025b)
 [33] M. Ghosh, M. Alam, *EPJ Web of Conf.* (2025c)